

Two-deuteron photodisintegration of ${}^4\text{He}$ at $E_\gamma=150\text{--}250$ MeV

B. J. Rice,* R. S. Canon, E. A. Wulf, and H. R. Weller

Triangle Universities Nuclear Laboratory and Duke University, Durham, North Carolina 27706

K. Keeter,† N. R. Kolb, C. Mueller, R. E. Pywell, G. A. Retzlaff, and D. M. Skopik

Saskatchewan Accelerator Laboratory, University of Saskatchewan, Saskatoon, Saskatchewan, Canada S7N 5C6

G. Feldman

Department of Physics, George Washington University, Washington, D.C. 20052

(Received 25 June 1999; revised manuscript received 15 February 2000; published 18 May 2000)

We have performed a measurement of the cross section for the ${}^4\text{He}(\gamma, dd)$ reaction with photon energies between 150 and 250 MeV. Both reaction particles were detected in coincidence. We obtained absolute cross sections at six angles and two energy bins (150–190 MeV and 190–250 MeV). A Legendre polynomial fit to the angular distribution shows a $\sin^2\theta$ distribution which suggests the isospin-forbidden $E1$ transition. However, a transition matrix element (TME) analysis using only strictly allowed transitions shows that the angular distribution can be described by just two TMEs: $E2$ s - and d -wave absorption on the D state of ${}^4\text{He}$. We performed an inverse direct-capture calculation in order to determine if the D state could contribute to such a high degree to the cross section. This calculation indicates that 90% of the cross section arises from absorption on the D state but fails to reproduce the observed $\sin^2\theta$ angular distribution.

PACS number(s): 25.20.-x, 23.20.En, 23.20.Js, 25.10.+s

I. INTRODUCTION

The ${}^4\text{He}$ system has been the subject of a great deal of experimental and theoretical study over the past 30 years (e.g., Ref. [1] and references contained therein). The observation of a nonzero tensor analyzing power T_{20} [2] indicated that the ${}^2\text{H}(d, \gamma){}^4\text{He}$ reaction is sensitive to the D state, and hence tensor force effects, in the ground state of ${}^4\text{He}$. Measurements of the ${}^2\text{H}(d, \gamma)$ reaction at deuteron energies below 80 keV [3,4] have yielded the unexpected (and unexplained) observation of p -wave strength in this system.

Since 1962, no less than five measurements of the ${}^4\text{He}(\gamma, dd)$ cross section have been attempted at or near $E_\gamma=200$ MeV [5–9]. These measurements show discrepancies of approximately three orders of magnitude in the total cross section. Furthermore, there are discrepancies in the shape of the angular distribution. Identical bosons in the exit channel and isospin selection rules would conspire to greatly limit $E1$ (and $M1$) radiation in this system with the result that one would expect electric quadrupole ($E2$) radiation to dominate. The characteristic shape of an $E2$ angular distribution is $\sin^2 2\theta$, which is peaked at 45° and 135° , and has a minimum at 90° .

The Arends [7] and Silverman [8] measurements suggest that the angular distribution is peaked at 90° in the center-of-mass frame and generally follows a $\sin^2\theta$ shape. This is intriguing because such an angular distribution shape is usually indicative of the dominance of electric dipole ($E1$) or magnetic dipole ($M1$) radiation. The apparent contradiction

between the naive theory and the results of these two measurements has generated some debate. Silverman [8] has suggested that the $E1$ shape implies the presence of meson-exchange current effects in this reaction. Another possibility involves D -state (tensor force) effects.

Discovering the true nature of the shape and magnitude of the cross section is the main motivation for the present work.

II. EXPERIMENTAL SETUP

The measurement was carried out using the tagged photon facility at the Saskatchewan Accelerator Laboratory (SAL). Electrons from the SAL pulse-stretcher ring (EROS) [10], with high duty factor (up to 90%), were directed onto a thin (115 μm thick) aluminum radiator. The 270 MeV primary electron beam was directed via a dump magnet into a well shielded beam dump. The bremsstrahlung photon beam passed through two collimators and a shielding wall before entering the experimental area. When photon tagging was employed, the postbremsstrahlung electrons were energy analyzed on the 62-channel focal plane of the photon tagging spectrometer. In this case there was also a coincidence requirement between a reaction product in the experiment and an electron on the focal plane, thus “tagging” the energy of the photon that initiated the reaction in the experiment. Complete details of the SAL tagged photon facility may be found in Ref. [11].

The tagger focal-plane detectors and electronics are limited to an average rate per tagger channel of approximately 1.5 MHz. This rate was not sufficient to allow this experiment to be carried out in a timely fashion due to the very small (~ 1 μb) total cross section for ${}^4\text{He}(\gamma, dd)$. Therefore the bulk of the data for this experiment was taken in an untagged bremsstrahlung mode at an equivalent average tagger channel rate of ~ 7.5 MHz. At this rate, the tagger focal-

*Present address: Intel Corporation, RA1-240, 5200 N.E. Elam Young Parkway, Hillsboro, OR 97124-6497.

†Present address: Department of Physics, Idaho State University, Pocatello, ID 83209-8106.

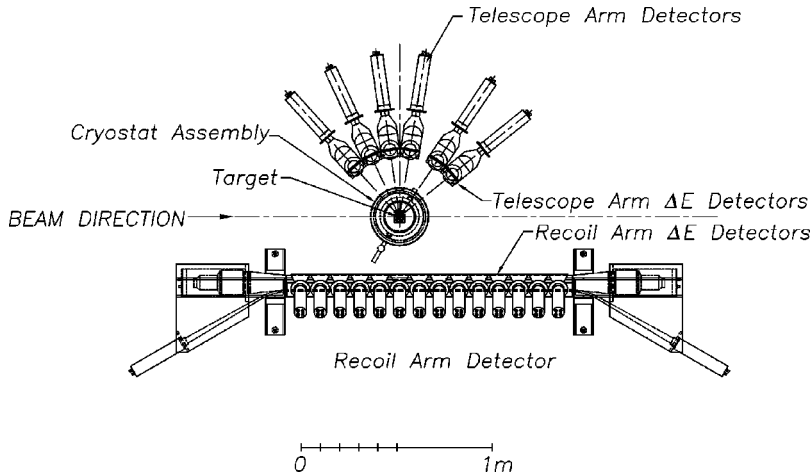


FIG. 1. Schematic of the experimental setup.

plane detectors had to be turned off. Therefore, to allow accurate flux normalization, two “beam current monitor paddles” (BCMPs) were positioned adjacent to the tagger focal-plane detectors. These paddles were narrow compared to the tagger detectors and thus the count rate in them was limited to an acceptable level during the high-flux untagged mode of operation. Several long tagged-photon runs and daily shorter tagged runs were performed at lower rates to allow cross-calibration of the photon flux between these BCMPs and the tagger counters. When tagged data were taken, the spectrometer was set to tag photons in the energy range 170 to 211 MeV.

When an electron was detected on the tagger focal plane, a corresponding bremsstrahlung photon was produced at the radiator. Not all of these photons reached the target due to the photon beam collimation. The fraction of photons that pass the collimators is called the tagging efficiency. This efficiency was measured at least once a day during the run by reducing the beam intensity by three orders of magnitude and counting the number of tagged photons passing through the collimators directly using a 100% efficient lead-glass detector. The tagging efficiency was about 65% and was shown to be stable during the course of the experiment. Variations of the order of 2% were accounted for in the analysis of the data.

The ^4He target was a liquid helium cell in the form of a 5 cm diameter vertical cylinder with 150 μm Mylar walls. This was placed inside an evacuated target chamber 25 cm in diameter, with thin Mylar windows in the directions of the detectors. The target cell was attached to the bottom of a liquid helium cryostat with a liquid nitrogen heat shield.

Figure 1 depicts the experimental layout showing the target and detector systems. One arm (the “telescope arm”) consisted of a set of six plastic scintillator telescopes placed at the angles $\theta_{\text{lab}} = 38.8^\circ, 55.0^\circ, 81.0^\circ, 98.1^\circ, 115.1^\circ,$ and 132.2° . Each telescope consisted of a ΔE - E detector pair. The E detectors were 10 cm \times 10 cm \times 7.6 cm (thick) plastic scintillator blocks and the ΔE detectors were 10 cm \times 10 cm \times 2 mm (thick) sheets of plastic scintillator. All were connected via light guides to 5 cm diameter photomultiplier tubes (PMTs). The solid-angle acceptance of each telescope was defined by a 35 mm diameter collimator placed in front of the ΔE detector. A Monte Carlo routine was used to cal-

culate the effective target length and the effective detector efficiency which is dependent on angle.

In order to ensure a full opening angle coverage, the other arm (the “recoil arm”) consisted of a single 1.5 m long \times 15 cm high \times 7.6 cm thick plastic scintillator bar viewed at each end by 12.5 cm diameter PMTs connected by lucite light guides. Providing segmentation in front of the bar were 14 plastic scintillator ΔE detectors, each 10 cm \times 10 cm \times 2 mm (thick), and behind the bar was a 1.5 m \times 15 cm \times 2 mm (thick) plastic scintillator “veto” detector viewed at each end by PMTs. This allowed the identification of high-energy particles that passed through the bar without depositing all their energy. The telescope arm determined the acceptance of the experiment, while the purpose of the recoil arm was to detect any coplanar particle in coincidence with a hit in the telescope arm.

All PMT signals were sent to constant fraction discriminators (CFDs). A valid hit in the telescope arm was defined as a hit in any of the six telescopes. A hit in an individual telescope was defined as a hit in the E detector plus a hit in the ΔE detector as well as the sum of the E plus ΔE signals passing a threshold (“sum threshold”) to reject electron hits. A valid hit in the recoil arm was defined as simply a coincidence between one of the 14 ΔE detectors and a hit in the E bar. A master trigger to read out the electronics was defined as a coincidence between a telescope arm hit and a recoil arm hit. In the case of tagged data, a hit on the tagger focal plane was also required.

All signals were sent to CAMAC modules which were read out through a parallel branch controlled by a MVME167 VME computer. This computer was in turn controlled by software running on a Sun Sparcstation computer connected via ethernet. Data were recorded on hard disk and ultimately written to CD for permanent storage. The whole system was controlled by the SAL data acquisition package LUCID [12].

III. DATA ANALYSIS

Deuterons in each detector arm were identified by means of a ΔE - E plot, an example of which is shown in Fig. 2. A linearized particle identification (PID) number was constructed by fitting the proton and deuteron ridges observed in

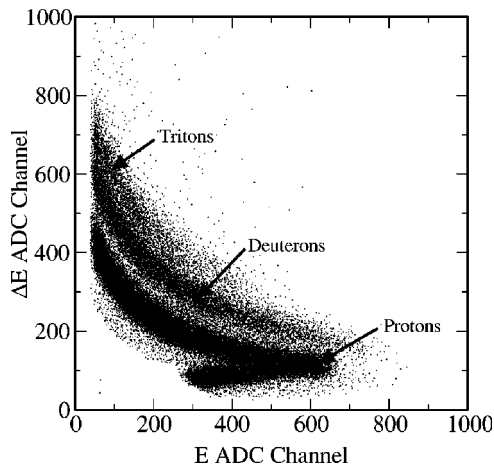


FIG. 2. Example ΔE - E plot for the telescope-arm detector at $\theta_{\text{lab}} = 38.8^\circ$. Clear separation of the proton and deuteron particle bands can be seen. The “bend-back” in the proton band where energetic protons punch through the back of the E scintillator can also be seen.

the ΔE - E plot. Examples of this PID parameter are shown for each arm in Fig. 3. The linearized PID made it possible to estimate, and correct for, the number of misidentified deuterons.

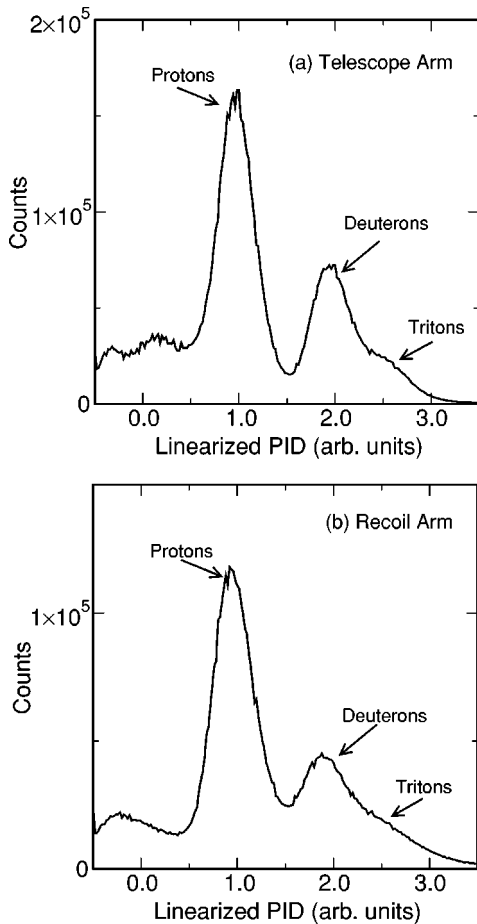


FIG. 3. Typical linearized PID spectra for the telescope arm (a) and recoil arm (b) detectors.

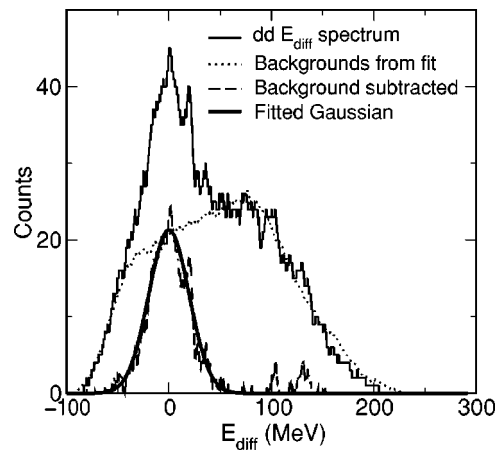


FIG. 4. E_{diff} spectrum for a typical telescope showing fitted background spectrum, the resulting dd spectrum and the Gaussian fit to the dd peak.

The energy calibration of all detectors was determined using the proton “bend-back” point observed in the ΔE - E plots (see Fig. 2). This is where an energetic proton punches through the back of the E scintillator. When this occurs, the energy deposited in the E scintillator can be calculated from the known energy loss of a proton in the scintillator material. From this, the light output in the scintillator can be calculated (using the method of O’Rielly [13]) and thus the response of the detector may be calibrated. In the experiment, this calibration and the calculated light output response were used to determine the particle energy deposited in each detector, and then an energy loss correction was made to deduce the particle energy at the interaction vertex.

Since the energies and angles of both detected deuterons were measured, the kinematics of the reaction was “overdetermined.” Using the angle and the energy determined in the recoil arm, and assuming both particles that passed a linearized PID cut were deuterons, the energy of the deuteron in the telescope arm was calculated. An energy difference, defined as the calculated energy in the telescope arm minus the measured energy ($E_{\text{diff}} = E_{\text{calc}} - E_{\text{meas}}$) was constructed, and is plotted for a typical telescope in Fig. 4. It can be seen that there is a large background of events mainly due to misidentified deuterons. These come from the large background of (γ, pt) , (γ, npd) and $(\gamma, ppnn)$ reactions. The shape of the contribution to the E_{diff} spectrum from each competing reaction channel was determined from the data by selecting each possible misidentified pair using the linearized PID. The shapes of these background E_{diff} spectra are therefore determined under identical experimental conditions as the (γ, dd) E_{diff} spectrum. A χ^2 fit was then made to the E_{diff} spectrum using these measured shapes for each background channel, and a Gaussian for the dd channel, to obtain the true (γ, dd) yield as shown in Fig. 4. The fitted gaussian for the dd channel was found to be centered around $E_{\text{diff}} = 0$ and has a width consistent with that estimated from the detector resolution found from the proton bandwidth. This indicates that the particle energy calibrations used were satisfactory. A correction was then made to this yield for the number of deuterons excluded in the initial cut in the PID spectrum. Two

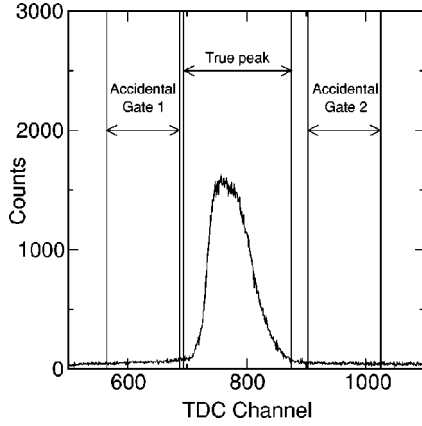


FIG. 5. Typical time difference spectrum between events in the recoil arm and events in the telescope arm. Shown are the “true” peak window and the windows used for fitting the accidental coincidence background.

methods were investigated for this correction, representing upper and lower bounds. The average result from these two methods was used to correct the data. This correction ranged from 9.4% to 17% depending on photon energy.

A correction of 7.5% was made to account for accidental coincidences between the two arms as determined from a TDC difference spectrum shown in Fig. 5. The error in the coincidence yield due to this correction was found to be less than 1%. Finally an empty target subtraction was made. Empty target runs were performed periodically during the experiment and these were analyzed using the same technique as for the full-target data. In the region of the dd peak in the E_{diff} spectrum this background was nearly flat and was about $20\% \pm 1\%$ of the full-target yield.

The data were grouped, according to reconstructed γ -ray energy, into two bins: a low-energy bin between 150 and 190 MeV and a high-energy bin between 190 and 250 MeV. Analysis of the ${}^4\text{He}(\gamma, pt)$ channel, measured in the same data taking run, show cross sections at the center-of-mass proton angles of 105° and 120° that agree well with previous measurements [14]. This gives us confidence that the absolute cross sections for this measurement are within the quoted systematic errors.

TABLE I. Differential cross sections for each telescope for the $E_\gamma = 150\text{--}190$ MeV bin and the $E_\gamma = 19\text{--}250$ MeV bin. Lab and center-of-mass angles are listed. The uncertainties listed are purely statistical and do not include a 7.1% systematic uncertainty for the low-energy bin and a 13% systematic uncertainty for the high-energy bin.

θ_{lab}	$E_\gamma = 150\text{--}190$ MeV		$E_\gamma = 190\text{--}250$ MeV	
	$\theta_{\text{c.m.}}$	$d\sigma_{\text{c.m.}}/d\Omega$ (nb/sr)	$\theta_{\text{c.m.}}$	$d\sigma_{\text{c.m.}}/d\Omega$ (nb/sr)
38.8°	44.7°	0.77 ± 0.15	45.4°	0.14 ± 0.11
55.0°	62.7°	1.26 ± 0.16	63.6°	0.59 ± 0.15
81.0°	90.3°	2.32 ± 0.20	91.4°	1.42 ± 0.17
98.1°	107.3°	1.73 ± 0.19	108.4°	1.11 ± 0.16
115.1°	123.5°	1.50 ± 0.17	124.4°	0.68 ± 0.12
132.2°	138.9°	1.03 ± 0.15	139.7°	0.43 ± 0.13

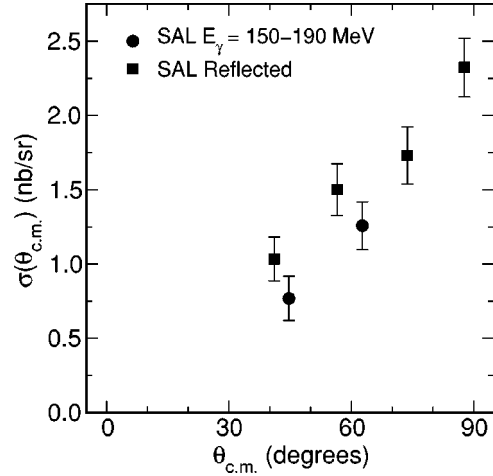


FIG. 6. SAL differential cross section for $E_\gamma = 150$ to 190 MeV. Exploiting the symmetry of the system, measured data (circles) with $\theta_{\text{c.m.}} > 90^\circ$ have been reflected about 90° and plotted (squares). The uncertainties shown are purely statistical and do not include a 7.1% systematic uncertainty.

IV. RESULTS

The resulting cross sections are presented in the center-of-mass frame and are listed in Table I. Since the exit channel of the reaction contains two identical particles, the cross section must be symmetric with respect to 90° in the center-of-mass. Accordingly, we have reflected the data about 90° . The resulting data sets are plotted in Fig. 6 and Fig. 7. We have found no evidence to suggest that the apparent asymmetry seen in Figs. 6 and 7 result from anything other than statistical uncertainty. There is a clear maximum at $\theta_{\text{c.m.}} = 90^\circ$ in the angular distributions for both the low-energy and high-energy data. Also shown in Fig. 7 are the measurements of Arends [7] and Silverman [8] at $E_\gamma = 213$ MeV.

A Legendre polynomial fit to the angular distribution data was performed using

$$\sigma(\theta_{\text{c.m.}}) = A_0 \left(1 + \sum_{k=1} Q_k a_k P_k(\cos \theta_{\text{c.m.}}) \right), \quad (1)$$

where $a_k = A_k/A_0$ and Q_k is a finite geometry correction factor [15]. The total cross section is $\sigma_{\text{tot}} = 2\pi A_0$ since there are

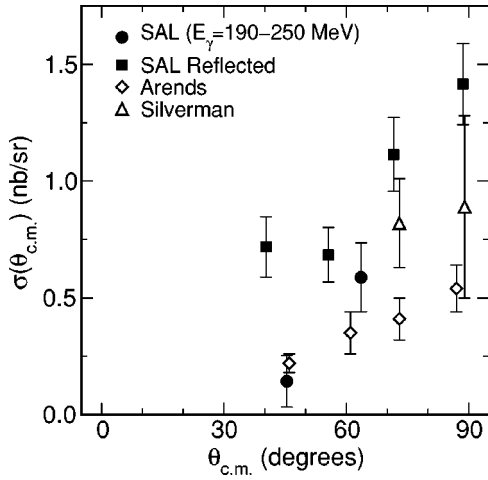


FIG. 7. SAL differential cross section for $E_\gamma = 190$ to 250 MeV. Exploiting the symmetry of the system, measured data (circles) with $\theta_{c.m.} > 90^\circ$ have been reflected about 90° and plotted (squares). The uncertainties shown are purely statistical and do not include a 13% systematic uncertainty. Also shown are the $E_\gamma = 213$ MeV data of Arends [7] (open diamonds) and Silverman [8] (open up triangles).

identical particles in the exit channel. The fit must be symmetric about 90° in the center-of-mass frame, therefore only even Legendre polynomials are included. A fit was constrained with the condition that the cross section be zero at 0° and 180° as done by Arends [7]. Another fit was performed without this constraint. Good fits were obtained with Legendre polynomials up to order $k=4$ and the results are presented in Table II and are plotted in Fig. 8. The angular distributions are consistent with a $\sin^2 \theta$ distribution rather than a $\sin^2 2\theta$ distribution. The a_4 coefficient is nonzero, even for the restricted fit for the high-energy data, indicating the possible presence of $E2$ or $M2$ radiation terms.

The total cross section values are assumed to lie between the results obtained from the constrained and unconstrained fits which do or do not include the P_4 terms. The difference between these fits was used to provide an estimate of the maximum systematic error on the total cross section values

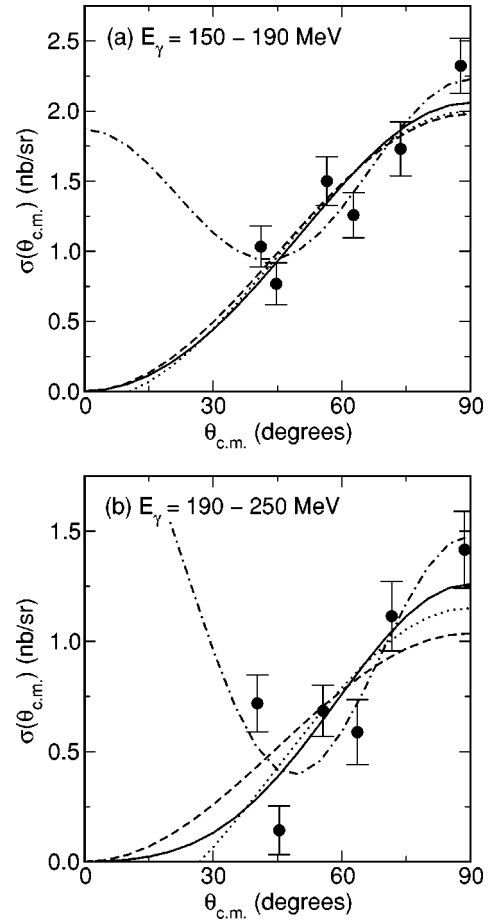


FIG. 8. Legendre polynomial fits to the angular distribution data. (a) shows the low-energy data ($E_\gamma = 150$ to 190 MeV) and (b) shows the high-energy data ($E_\gamma = 190$ to 250 MeV). In both (a) and (b) the fits are as follows: with P_0 and P_2 terms, constrained at $\theta_{c.m.} = 0^\circ$ and 180° to $\sigma = 0$, dashed line; with P_0 , P_2 , and P_4 terms, constrained, solid line; with P_0 and P_2 terms, unconstrained at $\theta_{c.m.} = 0^\circ$ and 180° , dotted line; with P_0 , P_2 , and P_4 terms, unconstrained, dot-dashed line.

TABLE II. Total cross sections and Legendre polynomial coefficients for the low- and high-energy bins. The first uncertainty on the total cross section is the statistical error from the fit, while the second represents the systematic uncertainty (7.1% for the low-energy bin, 13% for the high-energy bin). Fits are presented with the constraint that the cross section be zero at $\theta = 0^\circ$ and 180° , and without this constraint. Fits that exclude P_4 terms are also presented.

E_γ	Constraint	A_0	a_2	a_4	σ_{tot} (nb)
150–190 MeV	Constrained	1.32 ± 0.18	-1.08 ± 0.11	0.07 ± 0.09	$8.29 \pm 1.13 \pm 0.59$
150–190 MeV	Constrained	1.32 ± 0.06	-1.00 ± 0.05		$8.29 \pm 0.37 \pm 0.59$
150–190 MeV	Unconstrained	1.52 ± 0.13	-0.44 ± 0.28	0.68 ± 0.34	$9.55 \pm 0.82 \pm 0.68$
150–190 MeV	Unconstrained	1.31 ± 0.07	-1.06 ± 0.18		$8.32 \pm 0.40 \pm 0.65$
190–250 MeV	Constrained	0.71 ± 0.16	-1.33 ± 0.17	0.32 ± 0.14	$4.45 \pm 0.97 \pm 0.58$
190–250 MeV	Constrained	0.69 ± 0.05	-0.69 ± 0.05		$4.34 \pm 0.33 \pm 0.56$
190–250 MeV	Unconstrained	0.96 ± 0.11	-0.05 ± 0.34	1.13 ± 0.40	$6.05 \pm 0.67 \pm 0.79$
190–250 MeV	Unconstrained	0.67 ± 0.01	-1.45 ± 0.28		$4.20 \pm 0.03 \pm 0.55$

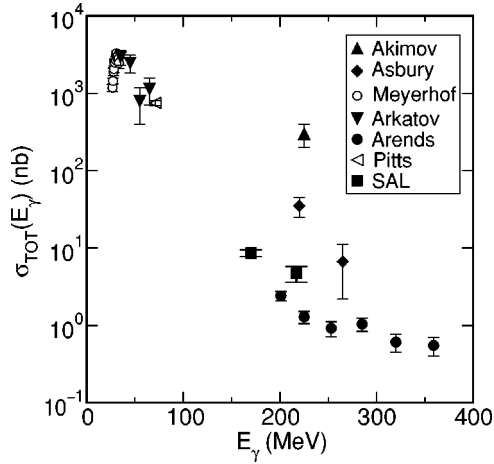


FIG. 9. World data for the total cross section compared with the results of the present measurements. Uncertainties for the present work represent the uncertainty in the Legendre polynomial fit to the data to obtain the total cross section combined with the systematic uncertainty (7.1% for the low-energy bin and 13% for the high-energy bin). Other data are from Akimov [5], Asbury [6], Meyerhof [16], Arkatov [17], Arends [7], and Pitts [18].

due to integration uncertainties. The results for the total cross section are presented in Fig. 9, along with the world data for ${}^4\text{He}(\gamma, dd)$ with E_γ greater than 30 MeV. The results are in agreement with those reported by Arends [7] to within about a factor of two. (Note that Arends's total cross section values were extracted from Legendre polynomial fits which were constrained to be zero at 0° and 180° .) Taken together, the weight of evidence from recent measurements indicates that the total cross section favors the lower values of those reported in the past 35 years.

V. TRANSITION MATRIX ELEMENT ANALYSIS

The ${}^4\text{He}(\gamma, dd)$ reaction is expected to be dominated by isoscalar $E2$ radiation, at least at relatively low energies [19]. The usually dominant $E1$ multipole is expected to be suppressed by spin and parity arguments. Since the outgoing deuterons are identical bosons, only outgoing states with $l+s$ even are allowed. This forbids $\Delta S=0$ $E1$ absorption, since $l=1$ is required in the outgoing channel (decay of a 1^- state), so that s must equal 1, while the ground state of ${}^4\text{He}$ has $L=0$, $S=0$ (S state), with a possible (small) $L=2$, $S=2$ (D state) admixture. The only allowed $E1$ transitions, therefore, correspond to $\Delta S=1$ $E1$ absorption leading to a 3p_1 final state (notation ${}^{2s+1}l_j$). Such strength, which is expected to be small, can result from coupled-channel effects, the spin-dependent part of the $E1$ operator, and tensor-force effects.

Since the absorption of $M1$ radiation leads to a 1^+ state, the outgoing channel must be a 5d_1 state in order to satisfy the $l+s$ even rule. This can only originate from the D -state component of the ground state, and is therefore expected to be small.

There are two possible outgoing channels for $M2$ absorption: 3p_2 and 3f_2 . Although magnetic strength is, in general,

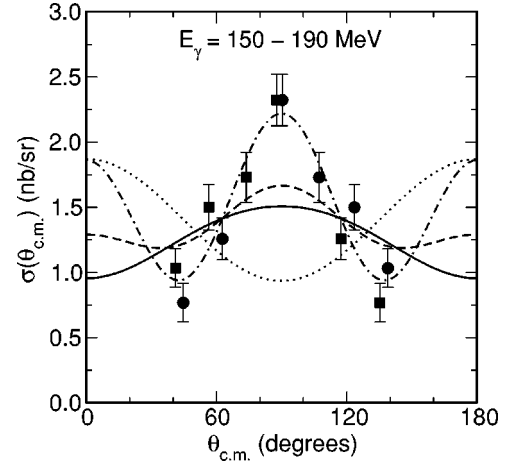


FIG. 10. Transition matrix element (TME) analysis results for the differential cross section at $E_\gamma=150$ to 190 MeV. Circles, SAL data; squares, reflected SAL data; dotted line, $E1$ only fit; solid line, $E2$ only fit; dashed line, $E1$, $E2$, and $M2$ fit; dot-dashed line, $E1$, $E2$, and $M2$ fit ignoring the constraint imposed by the analyzing power data (see text). Error bars shown are purely statistical.

expected to be smaller than electric strength of the same polarity by a factor of about 20 in the present case, these $M2$ amplitudes were included in the fit described below.

$E2$ absorption with $\Delta S=0$ on the S -state component of the ground state leading to a 2^+ state with $l=2$, $s=0$ is allowed and leads to an outgoing state which is 1d_2 . It is also possible to have $\Delta S=0$ $E2$ absorption on the D -state component of the ground state. This will lead to three possible outgoing channels: 5s_2 , 5d_2 , and 5g_2 , giving a total of four $E2$ outgoing amplitudes.

A transition matrix element (TME) analysis of the $E_\gamma=150$ – 190 MeV cross section data was performed using the formalism described by Weller *et al.* [20]. The fit made use of analyzing power data for the ${}^4\text{He}(\vec{\gamma}, dd)$ reaction obtained by the TUNL group at the Laser Electron Gamma Source (LEGS) at Brookhaven National Laboratory and reported in Ref. [21]. Although the information obtainable from this data was limited, it does indicate that the analyzing power is negative for photon energies between 185 and 310 MeV and for deuteron center-of-mass angles between 45° and 135° . This information was used to constrain the TME analysis fit.

This analysis included $E1$, $M1$, $M2$, and $E2$ absorption. As indicated above, this corresponds to eight transition matrix elements: ${}^3p_1(E1)$, ${}^5d_1(M1)$, ${}^3p_2(M2)$, ${}^3d_2(M2)$, ${}^1d_2(E2)$, ${}^5s_2(E2)$, ${}^5d_2(E2)$, and ${}^5g_2(E2)$. A χ^2 minimization was performed to simultaneously fit the cross section and analyzing power data. It was noticed that the $M1$ amplitude was negligible if any other multipole was included in the fit. Some of the fits to the angular distribution data are displayed in Fig. 10. It can be seen that there is a poor fit when only the $E1$ term is included. Reasonable fits were obtained when $E1$, $E2$, and $M2$ transitions were included. It is also interesting to observe that the assumption of $E2$ only transitions is capable of producing an angular distribution which is peaked at 90° , although not as strongly as the peaking observed in the data. The resulting amplitudes corre-

TABLE III. Amplitudes and phases from the transition matrix element (TME) analysis.

TME ${}^{2s+1}l_j$	$E1$ - $E2$ - $M2$ fit		$E2$ -only fit	
	Fraction of σ_{tot}	Rel. phase ($^\circ$)	Fraction of σ_{tot}	Rel. phase ($^\circ$)
1d_2 ($E2$)	0.000 ± 0.0012	-172.59 ± 360.00	0.000 ± 0.0008	-172.59 ± 360.00
5s_2 ($E2$)	0.745 ± 0.0339	0.00 ± 49.14	0.951 ± 0.0350	0.00 ± 34.06
5d_2 ($E2$)	0.013 ± 0.0083	0.00 ± 56.02	0.049 ± 0.0137	0.00 ± 31.05
5g_2 ($E2$)	0.000 ± 0.0000	0.00 ± 360.00	0.000 ± 0.0000	0.00 ± 360.00
3p_1 ($E1$)	0.090 ± 0.0255	0.00 ± 17.85		
3p_2 ($M2$)	0.091 ± 0.0304	0.00 ± 19.08		
3f_2 ($M2$)	0.061 ± 0.0310	0.00 ± 18.84		

sponding to both of these sets of assumptions are listed in Table III. A better fit to the cross section data may be obtained if the constraint imposed by the analyzing power data is ignored (as shown in Fig 10) however this fit fails to reproduce the analyzing power at $\theta_{\text{c.m.}}=90^\circ$. Under any circumstances, it was found that a reasonable fit to the cross section data that peaks at 90° can only be obtained if quadrupole terms are included.

As can be seen in Table III, the $E2$ -only fit places all the strength into $E2$ absorption on the D state of ${}^4\text{He}$ ($L=2$, $S=2$). This is somewhat surprising since the ($d+d$) D -state contribution has been determined to be only about 4% of the ground state of ${}^4\text{He}$ [19]. Furthermore, whereas lower-energy capture studies (corresponding to $E_\gamma=49$ MeV) have found significant g -wave strength, the present result indicates that the s -wave terms dominate in the $E_\gamma=150$ – 190 MeV region, with some d -wave admixture. It can also be observed that the s - and d -wave $E2$ ($S=2$) terms have the same phase (albeit with considerable errors), indicating that they interfere constructively. It is this constructive interference which gives rise to the observed maximum in the cross section at 90° .

Results from the $E1$ - $E2$ - $M2$ fit indicate that $E2$ absorption on the D state, leading to s - and d -wave outgoing amplitudes, is still present. In this case, however, spin-flip $E1$ ($S=0$ to $S=1$) and $M2$ absorption terms are also present. Constructive interference between the $E1$ and $M2$ terms, and between the $E2$ and $M2$ terms, contribute to the observed maximum at 90° in this case.

Looking at both fits, we can conclude that between 60% and 100% of the cross section arises from absorption on the D state of ${}^4\text{He}$. This absorption is dominated by $E2$ s waves (see Table III). Furthermore, the observed maximum in the cross section angular distribution at 90° arises from $E2$ (s wave)- $E2$ (d wave), $E2$ - $M2$, and/or $E1$ - $M2$ constructive interference.

VI. DIRECT CAPTURE CALCULATIONS

Direct capture (DC), or, shall we say, direct photodisintegration in the present case, is expected to be the dominant mechanism in this reaction at very low center-of-mass energies. In the case of capture reactions using incident deuteron energies as high as 50 MeV ($E_\gamma \sim 50$ MeV), the DC model has been shown to reproduce the observed cross sections and

analyzing powers with reasonable success [19]. However, as the deuteron or γ -ray energy increases, the usefulness of the DC model becomes limited. For example, in the work of Pitts *et al.* [18] at a deuteron energy of 95 MeV ($E_\gamma \sim 70$ MeV), the direct capture model failed to predict even the correct sign of the tensor analyzing power A_{yy} .

For the present case, the direct photodisintegration calculations were performed using the parameters from Ref. [19]. This included an optical model potential used to describe the outgoing scattering state [obtained from fitting 30 and 50 MeV elastic scattering data from the ${}^2\text{H}(d, \gamma){}^2\text{H}$ reaction], and the Woods-Saxon well parameters used to generate the S - and D -wave two point-deuteron ground-state wave functions for the target nucleus ${}^4\text{He}$. Since the lower-energy work indicated a $d+d$ D -state probability in the ground state of ${}^4\text{He}$ of 4%, this value was also used in the present case. The calculations were performed using the full Bessel function forms of the electric multipole operators.

Overall, the results of the DC calculation which included $E2$ and spin-flip $E1$ transitions failed to describe the present data. The calculations did not predict an angular distribution for the cross section which is peaked near 90° . This resulted from the fact that, unlike the results of the TME analysis which predicted predominantly s -wave emission, the DC calculation indicated that g waves would dominate. Unless the optical potentials were drastically altered, the calculation failed to reproduce the measured absolute cross sections. However, the calculations did indicate that, even though the D state in the ground state of ${}^4\text{He}$ had only a 4% probability, $E2$ photoabsorption on the D state was responsible for more than 90% of the cross section in the $d+d$ channel, as found in the TME analysis. Overall, it is clear that the DC model is entirely too simplistic and fails to describe the situation at the present energies.

VII. CONCLUSIONS

We have measured angular distributions for the ${}^4\text{He}(\gamma, dd)$ reaction in the two energy bins $E_\gamma=150$ – 190 MeV and $E_\gamma=190$ – 250 MeV.

A transition matrix element analysis of the data including $E1$, $M1$, $E2$, and $M2$ multipole transitions was performed. This analysis found that between 60% and 100% of the cross section arises from absorption on the D state of ${}^4\text{He}$ with the dominant contribution coming from s -wave absorption. Fur-

thermore, it was found that the maximum in the cross section angular distribution at 90° is a consequence of $E2(s\text{ wave})$ - $E2(d\text{ wave})$, $E1$ - $M2$, and $E2$ - $M2$ constructive interference.

The absolute total cross section for ${}^4\text{He}(\gamma, dd)$ for E_γ near 220 MeV favors the lower values of those published during the last 35 years. We feel that the cross section is now known to within $\sim 30\%$, as opposed to within a factor of 100 or 1000.

The angular distribution was found in this work to be maximum at 90° , in agreement with the Arends [7] and Silverman [8] measurements. The first observation of this result sparked debate because such an angular distribution is normally associated with $E1$ radiation [8], whereas $E2$ transitions were expected to dominate this reaction. Such angular distributions typically exhibit a $\sin^2 2\theta$ shape which has a minimum at 90° and maxima near 45° and 135° . This inconsistency caused Silverman [8] to suggest that the shape of the angular distribution arose from $E1$ radiation coming from meson-exchange currents. The isoscalar nature of both the deuteron and ${}^4\text{He}$, however, makes such exchange currents

unlikely. In this work, we have shown that it is, in fact, possible to create an angular distribution that is peaked at 90° using $E2$ s -wave absorption on the D state interfering constructively with $E2$ d -wave absorption on the D state, or with $M2$ radiation. $M1$ - $E2$ constructive interference can also contribute to this shape.

These observations indicate the vital importance of the tensor force in the present system. The possibility that it plays a dominant role at such high energies is quite intriguing. We hope that this interesting result will motivate the four-body theorists to investigate this physics-rich reaction at these energies in the near future.

ACKNOWLEDGMENTS

This work was supported in part by the U.S. Department of Energy under Contract No. DE-FG02-97ER41033, and in part by a grant from the Natural Sciences and Engineering Research Council of Canada.

-
- [1] J. M. Laget, Nucl. Phys. **A579**, 333 (1994).
 - [2] H. R. Weller, P. Colby, N. R. Roberson, and D. R. Tilley, Phys. Rev. Lett. **53**, 1325 (1984).
 - [3] L. H. Kramer, Ph.D. thesis, Duke University, 1992.
 - [4] L. H. Kramer, R. M. Chasteler, E. Hayward, R. M. Prior, D. R. Tilley, and H. R. Weller, Phys. Lett. B **304**, 208 (1993).
 - [5] Yu. K. Akimov, O. V. Savchenko, and L. M. Sorok, Zh. Éksp. Teor. Fiz. **41**, 708 (1961) [Sov. Phys. JETP **14**, 512 (1962)].
 - [6] J. G. Asbury and F. J. Loeffle, Phys. Rev. **137**, B1214 (1965).
 - [7] J. Arends, J. Eyink, T. Hegerath, B. Mecking, G. Nöldeke, and H. Rost, Phys. Lett. **62B**, 411 (1976).
 - [8] B. H. Silverman, A. Boudard, W. J. Briscoe, G. Bruge, P. Couvert, L. Farvarque, D. H. Fitzgerald, C. Glashauser, J.-C. Lugal, and B. M. K. Nefkens, Phys. Rev. C **29**, 35 (1984).
 - [9] G. V. O’Rielly, Ph.D. thesis, University of Melbourne, 1997.
 - [10] L. O. Dallin, Ph.D. thesis, University of Saskatchewan, 1990.
 - [11] J. M. Vogt, R. E. Pywell, D. M. Skopik, E. L. Hallin, J. C. Bergstrom, H. S. Caplan, K. I. Blomqvist, W. Del Bianco, and J. W. Jury, Nucl. Instrum. Methods Phys. Res. A **324**, 98 (1993).
 - [12] Saskatchewan Accelerator Laboratory Report, ‘‘LUCID User’s Guide,’’ 1995 (unpublished).
 - [13] G. V. O’Rielly, N. R. Kolb, and R. E. Pywell, Nucl. Instrum. Methods Phys. Res. A **368**, 745 (1996).
 - [14] C. Mueller, M.Sc. thesis, University of Saskatchewan, 1999.
 - [15] M. E. Rose, Phys. Rev. **91**, 610 (1953).
 - [16] W. E. Meyerhof, W. Feldman, S. Gilbert, and W. O’Connell, Nucl. Phys. **A131**, 489 (1969).
 - [17] Y. M. Arkatov, P. I. Vatsset, V. I. Voloshchuk, I. M. Prokhorets, A. F. Khodyachikh, and V. I. Chmil, Yad. Fiz. **11**, 1172 (1974) [Sov. J. Nucl. Phys. **19**, 598 (1974)].
 - [18] W. K. Pitts, H. O. Meyer, L. C. Bland, J. D. Brown, R. C. Byrd, M. Hugi, H. J. Karwowski, P. Schwandt, A. Sinha, J. Sowanski, and I. J. van Heerden, Phys. Rev. C **39**, 1679 (1989).
 - [19] R. M. Whitton, H. R. Weller, E. Hayward, W. R. Dodge, and S. E. Dodge, Phys. Rev. C **48**, 2355 (1993).
 - [20] H. R. Weller, J. Langenbrunner, R. M. Chasteler, E. L. Tomusiak, J. Asai, R. G. Seyler, and D. R. Lehman, At. Data Nucl. Data Tables **50**, 29 (1992).
 - [21] B. J. Rice, Ph.D. thesis, Duke University, 1998.